Tetradentate Macrocyclic Complexes of Platinum. Evaluation of the Stereochemical Alterations of Redox Behavior and the X-ray Crystal Structure of (1,4,7,10-Tetrathiacyclodecane)platinum(II) Chloride

Murielle A. Watzky,[1a] David Waknine,[1a] Mary Jane Heeg,[1a] John F. Endicott,*[1a] and L. A. Ochrymowyzc[1b]

Departments of Chemistry, Wayne State University, Detroit, Michigan 48202, and University of Wisconsin—Eau Claire, Eau Claire, Wisconsin 57401

Received March 10, 1993®

The X-ray crystal structure of $Pt([12]aneS_4)^{2+}$ ([12]aneS$_4$ = 1,4,7,10-tetrathiacycloduodecane) shows that the Pt(II) ion is displaced 0.33 Å from the S$_4$ plane but that the Pt–S bond length is 2.29 Å, the same as found earlier (Waknine *et al. Inorg. Chem.* **1991**, *30*, 3691) for $Pt([14]aneS_4)^{2+}$ ([14]aneS$_4$ = 1,4,8,11-tetrathiacyclotetradecane). This bond length is about 0.04 Å shorter than expected on the basis of comparisons of covalent radii and on the basis of Cu–S bond lengths found for Cu(II) complexes with the same ligands. The shortened Pt–S bond suggests a relatively large π-back-bonding contribution from the electron-rich Pt(II) to the sulfur ligand. The increasingly positive potential for the two-electron electrochemical oxidation of the $Pt([n]aneS_4)^{2+}$ complexes in chloride media as *n* decreases from 16 to 14 (Waknine *et al.*) has been shown by molecular mechanics calculations to originate mostly from the stereochemical repulsions between axial chloride in the Pt(IV) product and the equatorial [*n*]aneS$_4$ ligand. A component of the observed electrochemical shifts appears to arise from the varying angular disposition of the π-acceptor orbitals of the bonding S atoms as the ring size is changed. These varying angular, or "electronic", components of the Pt–S bond also result in substantial changes in the energies and intensities of the lowest energy metal-centered transitions. $[Pt([12]aneS_4)]Cl_2 \cdot H_2O$ crystallizes in the tetragonal space group $P4/n$ with $Z = 2$, $a = b = 10.8760$ (9) Å, and $c = 7.830(2)$ Å. The structure refined to $R = 0.023$ and $R_w = 0.028$ for 793 unique, observed reflections.

Introduction

Macrocyclic ligands can be used to systematically alter the kinetic and thermodynamic factors which determine the patterns of transition metal reactivity.[2-6] In a recent report[7] we proposed that the variations observed for the Pt(II)/Pt(IV) redox couples of certain complexes containing tetradentate macrocyclic ligands most probably arose from alterations of stereochemical contributions to the differences in stabilities of the respective 4- and 6-coordinate complexes. The potential for stereochemical perturbations of the stability of Pt(IV) complexes was illustrated by the structure of $Pt([14]aneS_4)^{2+}$,[7,8] in which the tetrathioether ligand was not symmetrically coordinated; rather, it was folded so that the four chelate rings were near the same axial site of the metal. 6-Coordination in such a complex should result in appreciable stereochemical repulsions between an axial ligand and the neighboring chelate rings. The stereochemical effects of macrocyclic ligand folding are expected to increase in significance as the macrocyclic ring size is decreased. In order to further explore this argument, we have synthesized the platinum(II) complex containing the relatively small [12]aneS$_4$[8] (see Figure 1) macrocyclic ligand. This complex and its X-ray crystal structure are reported in this paper. We have also used molecular mechanics calculations to examine more critically the contributions of stereochemical factors to the redox behavior of $Pt([n]aneS_4)^{2+}/Pt([n]aneS_4)Cl_2^{2+}$ couples. This more detailed analysis, combined with variations in the electronic absorption spectra suggests that electronic factors associated with variations in metal–ligand bonding may also play a significant role in the redox chemistry of these complexes.

Experimental Section

Materials. The literature procedure was used for synthesis of the complexes,[7] with the modifications indicated below. The cyclic thioether ligands have been reported in studies from Professor D. B. Rorabacher's laboratory,[9] and their synthesis is reported elsewhere.

$[Pt([12]aneS_4)](PF_6)_2$. A 0.25-mmol sample of K_2PtCl_4 and 0.275 mmol of the ligand were combined in a 1:4 (v/v) mixture of DMSO and CH_3CN at 50 °C, and the mixture was refluxed for 2 h. A yellow, clear solution was obtained. After this solution was cooled, Et_2O was added and a golden, shiny precipitate was formed. It was further recrystallized in a saturated solution of NH_4PF_6 for analysis. Anal. Found (calcd) for $C_8H_{16}S_4F_{12}P_2Pt$: C, 13.21 (13.24); H, 2.22 (2.22); S, 17.97 (17.68); P, 8.34 (8.54).

$[Pt([13]aneS_4)](PF_6)_2$. The reactants were dissolved in the solvent mixture, and the solutions were deaerated in separate vessels; then they were combined slowly and anaerobically (N_2 purge). Heating was started during this addition, and the reaction mixture was refluxed at 80–100 °C for about 15 h. A pale yellow suspension was formed on cooling. The product was decanted and then filtered. It was then dissolved at 60–80 °C in a large excess of H_2O, and a pale yellow precipitate was formed by adding an excess of NH_4PF_6 at that temperature. The yield was 41%. Anal. Found (calcd) for $C_9H_{18}S_4F_{12}P_2Pt$: C, 14.94 (14.61); H, 2.65 (2.43); S, 16.99 (17.32); P, 8.41 (8.39).

* Abstract published in *Advance ACS Abstracts*, October 1, 1993.

(1) (a) Wayne State University. (b) University of Wisconsin-Eau Claire.

(2) Melsen, G. A., Ed. *Coordination Chemistry of Macrocyclic Compounds*; Plenum: New York, 1979.

(3) Lindoy, L. F. *The Chemistry of Macrocyclic Ligand Complexes*; Cambridge University Press: Cambridge, U.K., 1989.

(4) Bernal, I. *Stereochemistry and Stereophysical Behavior of Macrocycles*; Elsevier: Amsterdam, 1987.

(5) Hancock, R. D.; Martell, A. E. *Chem. Rev.* **1989**, *89*, 1875.

(6) Blake, A. J.; Schroder, M. *Adv. Inorg. Chem.* **1990**, *35*, 2.

(7) Waknine, D.; Heeg, M. J.; Endicott, J. F.; Ochrymowycz, L. A. *Inorg. Chem.* **1991**, *30*, 3691.

(8) Ligand abbreviations: [12]aneS$_4$ = 1,4,7,10-tetrathiacycloduodecane; [13]aneS$_4$ = 1,4,7,10-tetrathiacyclotridecane; [14]aneS$_4$ = 1,4,8,11-tetrathiacyclotetradecane; [15]aneS$_4$ = 1,4,8,12-tetrathiacyclopentadecane; [16]aneS$_4$ = 1,5,9,13-tetrathiacyclohexadecane; [9]aneS$_3$ = 1,4,7-trithiacyclononane; [9]aneN$_3$ = 1,4,7-triazacyclononane; [14]aneN$_4$ = 1,4,8,11-tetrathiacyclotetradecane.

(9) Pett, V. B.; Diaddario, L. L.; Dockal, E. R.; Corfield, P. W.; Ceccarelli, C. L.; Glick, M. D.; Ochrymowycz, L. A.; Rorabacher, D. B. *Inorg. Chem.* **1983**, *22*, 3661.

0020-1669/93/1332-4882$04.00/0

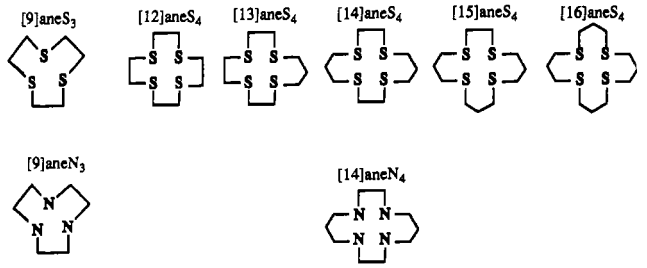

Figure 1. Skeletal structures of macrocyclic ligands.

The other complexes were prepared using minor variations of this procedure.

[Pt([14]aneS$_4$)]Cl$_2$. The reaction mixture was refluxed for 20 min.

[Pt([15]aneS$_4$)]Cl$_2$. A white crystalline solid was prepared using the literature procedure.[7]

[Pt([16]aneS$_4$)](PF6)$_2$. A pale yellow crystalline solid was obtained using the procedure for [Pt([13]aneS$_4$)](PF$_6$)$_2$. It turned white after recrystallization with NH_4PF_6. The yield was 54%. Analysis Found (calcd) for $C_{12}H_{24}S_4F_{12}P_2Pt$: C, 17.93 (18.43); H, 3.00 (3.07).

General Techniques. Elemental analyses were obtained from Midwest Microanalytical Laboratories. Visible–UV spectra were taken on an OLIS modified Cary 14 spectrophotometer. ^{1}H NMR spectra were obtained on a Nicolet QE-300 instrument.

Electrochemical Techniques. Cyclic voltammetry was performed on a Princeton Applied Research (PAR) Model 173 potentiostat/galvanostat, equipped with a PAR Model 179 digital coulometer and a PAR Model 175 universal programmer, together with a Nicolet Model 206 oscilloscope. A platinum disk working electrode and Ag/AgCl reference were used. The electrolytic medium was 0.1 M LiCl in a mixture of CH_3CN and H_2O (4:1, v/v). Complex concentrations were about 10^{-4}–10^{-3} M. The solutions were deaerated under N_2, and the working electrode was washed with HNO_3 between scans. Ferrocene was used as an internal standard, and it was assumed that $E°(Fe/Fe^+) = +0.36$ V (vs Ag/AgCl)[10] under the experimental conditions.

All the Pt complexes were found to adsorb onto the platinum electrode surface (adsorption was indicated by nonproportionality of the peak intensities to the square root of the scan rate and by shifts of the half-wave potentials).[10] The system response was sensitive to the conditions under which the experiment was made. For the most reproducible results, the electrode was pretreated by taking repeated scans in a solution of a different Pt complex, in order to create a coat on the surface. The same results were obtained with any complex, as long as it was not the one under investigation. Prior to this pretreatment, the electrode was polished with Buehler's Metadi (6 and 1 μm) and Micropolish (0.3 and 0.05 μm) polishing compounds. The results were considered satisfactory when the peak intensities varied in direct proportion to the square root of the scan rate ($i \propto v^{1/2}$).

Molecular Mechanics. A version of Allinger and Yuh's MM2,[11] modified as described elsewhere,[12] was used on a VAX 11/750 computer. The Urey–Bradley force field (UBFF) can be expressed in terms of its components: $U_{UB} = U_{str} + U_{bend} + U_{str-bend} + U_{vdW} + U_{torsion} + U_{dipole}$.

Stretch–bend contributions involving Pt were set to zero. Stretching and bending parameters, as well as dipoles, needed to be set for Pt, or to be adjusted for S. A detailed description of the input parameters can be found in Table S-I of the supplementary material.[13] Trial coordinates were derived from the X-ray data available for [Pt([12]aneS$_4$)]X$_2$ and [Pt([14]aneS$_4$)]X$_2$. Atoms were added or withdrawn, when needed to create the other macrocyclic ligands. Due to the shallowness of the potential surfaces of these systems, we were concerned that local minima might be generated. We attempted to circumvent this problem by scanning a range of trial geometries. Calculated bond lengths and angles can be compared to the X-ray data available. The data fit is reasonable, and can be found in Tables S-II and S-III of the supplementary material.[13] Figures were drawn using Schlegel's model software.

(10) Bard, A. J.; Faulkner, L. R. *Electrochemical Methods. Fundamentals and Applications*; Wiley: New York, 1980.
(11) Allinger, N. L.; Yuh, Y. H. Quantum Chemistry Program Exchange, Indiana University, Bloomington, IN; Program No. 395.
(12) (a) Perkovic, M. W.; Heeg, M. J.; Endicott, J. F. *Inorg. Chem.* **1991**, *30*, 3140. (b) Perkovic, M. W. Ph.D. Dissertation, Wayne State University, 1990.
(13) See paragraph at end of paper regarding supplementary material.

Table I. Crystallographic Data for [Pt([12]aneS$_4$)]Cl$_2$·H$_2$O

formula	$PtCl_2S_4O_4C_8H_{24}$	fw	578.53
$a = b$	10.8760(9) Å	space group	$P4/n$ (No. 85)[b]
c	7.830(2) Å	λ	0.710 73 Å
V	926.2(3) Å^3	ρ(calc)	2.074 g cm^{-3}
Z	2	μ	83.83 cm^{-1}
R^a	0.023	transm coeff	0.063–0.023
$R_w{}^a$	0.028	T	22 °C

[a] $R = (\Sigma||\Delta F|)/\Sigma|F_o|$; $R_w = [(\Sigma w|\Delta F|^2)/\Sigma wF_o^2]^{1/2}$. [b] The origin was chosen to coincide with the inversion center.

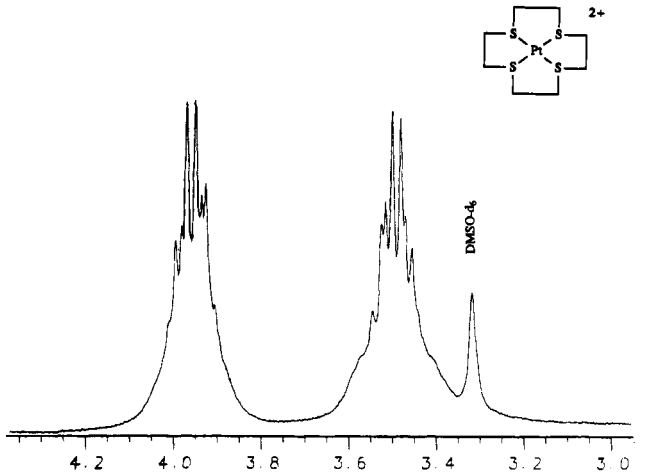

Figure 2. ^{1}H NMR spectrum of [Pt([12]aneS$_4$)](PF$_6$)$_2$ in DMSO-d_6. Horizontal scale is ppm vs TMS.

Table II. Absorption Data for Macrocyclic Platinum(II) Complexes

complex	λ_{max} (nm) [ϵ (M^{-1} cm^{-1})]
[Pt([12]aneS$_4$)]Cl$_2$[a]	207 [13 863]; ~220[sh,d] 286.5 [3516]; 341 [1941]
[Pt([13]aneS$_4$)](PF$_6$)$_2$[b]	205 [18 727]; 220.5 [13 251]; 276.5 [4312]; 327 [1848]
[Pt([14]aneS$_4$)]Cl$_2$[a]	205.5 [17 951]; 218 [15 639]; ~235[sh]; 262.5 [3386]; 315 [1195]
[Pt([15]aneS$_4$)]Cl$_2$[a]	211.5 [9769]; 229.5 [14 892]; ~260[sh]; 321 [579]
[Pt([16]aneS$_4$)](PF6)$_2$[b]	~215[sh]; 234 [16 701]; ~270[sh]; 327.5 [467]
[Pt([14]aneN$_4$)]Cl$_2$[a]	211 [6328]; 232.5 [442]; 264 [77]
[Pt(NH$_3$)$_4$](ClO$_4$)$_2$[c]	197 [11 070]; 221[sh]; 240[sh]; 286 [42.5][a] 198 [12 300]; 217 [560]; 232[sh]; 289 [54][b]

[a] In H_2O. [b] In CH_3CN. [c] Mason, W. R.; Gray, H. B. *J. Am. Chem. Soc.* **1968**, *90*, 5721. [d] Shoulder; peak not resolved.

Crystallography. [Pt([12]aneS$_4$)]Cl$_2$·H$_2$O. The single-crystal X-ray diffraction experiment was performed on a Nicolet R3 automated diffractometer with Mo Kα radiation (λ = 0.710 73 Å) and a graphite monochromator at ambient temperature. The structure was solved by Patterson methods and refined in a full matrix with the programs of SHELX-76.[14] Neutral-atom scattering factors and corrections for anomalous dispersion were taken from ref 15. Tabular crystallographic data are presented in Table I and in the supplementary material.[13] Absorption corrections were derived empirically from ψ scans.

Results

The ^{1}H NMR spectrum of Pt([12]aneS$_4$)$^{2+}$ is represented in Figure 2. The Pt^{II} thioether complexes have also been characterized by visible–UV absorption. Absorption maxima and extinction coefficients are given in Table II. Due to the uncertainty in the number of overlapped peaks, the spectra have not been deconvoluted; absorptivities were calculated from the apparent intensities. No significant (±1 nm) shift of the absorption maxima

(14) Sheldrick, G. M. SHELX-76. University Chemical Laboratory, Cambridge, England, 1976.
(15) *International Tables for X-ray Crystallography*; Kynoch Press: Birmingham, England, 1974; Vol. IV (present distributor D. Reidel, Dordrecht, The Netherlands).

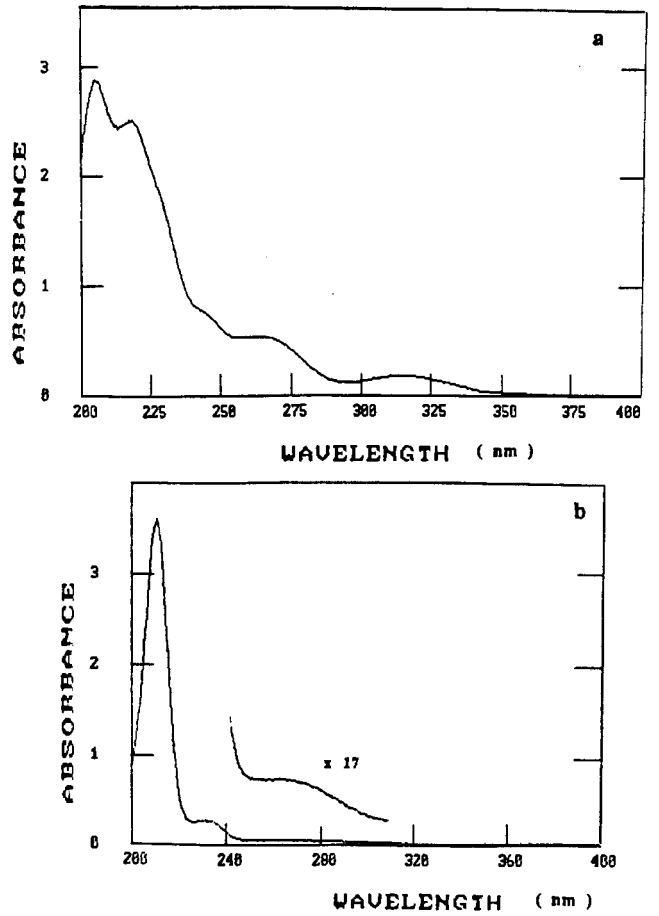

Figure 3. Absorption spectra of $[Pt([14]aneS_4)]Cl_2$ (a) and $[Pt([14]aneN_4)Cl_2$ (b) in water at 25 °C.

Table III. Redox Potentials of the Pt(II/IV) Couple in Macrocyclic Thioether Complexes[a]

complex	scan rate (mV/s)	$E_{1/2}$ (V)	ΔE_p (mV)
$[Pt([14]aneS_4)]Cl_2$	496	0.812	231
	198	0.799	144
	99	0.797	127
$[Pt([15]aneS_4)](PF_6)_2$	497	0.737	191
	199	0.731	142
	99	0.729	131
$[Pt([16]aneS_4)](PF_6)_2$	496	0.678	158
	198	0.674	126
	99	0.673	109

[a] Vs Ag/AgCl in 0.1 M LiCl in 80% CH_3CN–20% H_2O.

was observed by changing the solvent from water to acetonitrile; nor were any shifts observed by changing the counterion from Cl^- to PF_6^-. No absorption was detected in the 400–800-nm region ($\epsilon \leq 10^2$ M^{-1} cm^{-1}). For comparison, the spectra of $[Pt([14]aneN_4)]Cl_2$ and $[Pt([14]aneS_4)]Cl_2$ are shown in Figure 3. Additional spectra can be found in Figures S-1–S-4 of the supplementary material.[13]

Electrochemistry. The reactions $\{Pt([n]aneS_4)^{2+} + 2Cl^- \rightleftharpoons Pt([n]aneS_4)Cl_2^{2+} + 2e^-\}$ are quasi-reversible. The redox potentials ($E_{1/2} = [E_{p_a} + E_{p_c}]/2$) of the Pt(II/IV) couple in $Pt([14]aneS_4)^{2+}$, $Pt([15]aneS_4)^{2+}$, and $Pt([16]aneS_4)^{2+}$ complexes are reported in Table III. We were not able to determine the half-wave potential for $Pt([13]aneS_4)^{2+}$ or $Pt([12]aneS_4)^{2+}$ complexes. For these complexes, the oxidation and reduction waves were probably hidden by those of the O_2/H_2O ($E_{1/2}$ = +1.032 V vs Ag/AgCl)[10] and Cl_2/Cl^- ($E_{1/2}$ = +1.161 V vs Ag/AgCl) couples. Within the experimental conditions, the limit of observable potentials is estimated to be ≤0.9 V (vs Ag/AgCl).

Molecular Mechanics. The configurations of minimum steric energy have been determined for the $Pt([n]aneS_4)^{2+}$ and $Pt([n]aneS_4)Cl_2^{2+}$ complexes, where n = 12–16. Some Pt(II) complexes for which no crystallographic structure is known are represented in Figure 4. MM2 calculations on the Pt(II) to Pt(IV) complexes found that the Pt atom moved into the macrocyclic ring and that the ring flattened on forming the 6-coordinate Pt(IV) complex. The change was more dramatic as the size of the ring decreased, as illustrated in Figure 6a. Details of the calculated steric energies are presented in Table IV. The calculated steric energies of the $Pt(S_4)^{2+}$ complexes show a minimum at $Pt([14]aneS_4)^{2+}$, while, for the Pt(IV) complexes, they approach a constant value at $Pt([15]aneS_4)Cl_2^{2+}$. The steric energy differences are plotted vs $E_{1/2}$ in Figure 8.

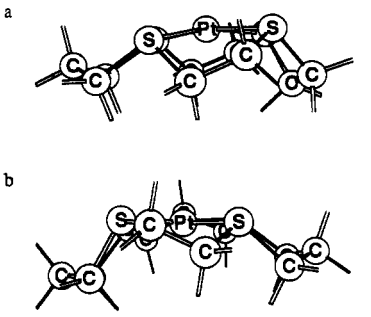

Figure 4. Steric energy minimized geometries of $Pt([13]aneS_4)^{2+}$ (a) and $Pt([15]aneS_4)^{2+}$ (b).

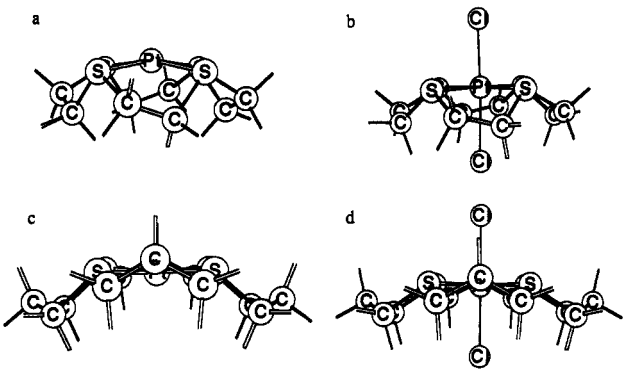

Figure 5. Steric energy minimized geometries of $Pt([n]aneS_4)^{2+}$ and $Pt([n]aneS_4)Cl_2^{2+}$ for n = 12 (a and c) and 16 (b and d). Note that the Pt is out of the S_4 plane in $Pt([12]aneS_4)$, but in the plane in $Pt([n]aneS_4)Cl_2^{2+}$, and that the $(CH_2)_n$ backbones of both rings are somewhat displaced to accommodate 6-coordination.

Crystallography. $[Pt([12]aneS_4)](Cl)_2 \cdot H_2O$. The atomic fractional coordinates are presented in Table V. Bond lengths and angles are given in Table VI. Figure 7 shows diagrams of the cation illustrating the geometry and labeling scheme. The Pt atom occupies a 4-fold rotation axis, as does one of the Cl^- anions (Cl2). The other Cl^- anion (Cl1) occupies a $\bar{4}$ symmetry site. Other atoms are on general positions in the cell. Although no hydrogen atoms were placed on the solvent water molecule, close contacts between O1 and S1 (3.15 Å), O1 and Cl1 (3.19 Å), and O1 and Cl2 (3.24 Å) indicate a hydrogen-bonding network in the lattice. The sulfur atoms in the $[12]aneS_4$ macrocycle are necessarily planar by symmetry; the Pt atom is 4-coordinate and lies only 0.33 Å out of the S_4 plane. The ligand is configured so that lone pairs on all four sulfur donor atoms would be oriented similarly: all atoms of the macrocycle lie on one side of the S_4 plane. The closest atomic contact of Pt is to C12′ directly in an axial position on the open face at 3.312 Å. The four Pt–S bonds are crystallographically equal at 2.293(1) Å.

Discussion

The $Pt([12]aneS_4)^{2+}$ structure represents important and surprising features in the study of macrocycle ring size effects. This laboratory recently published the electrochemistry and crystal structures of a number of similar Pt macrocyclic complexes,

Table IV. Calculated Steric Energies for $Pt([n]aneS_4)^{2+}$ and $Pt([n]aneS_4)Cl_2^{2+}$ Complexes[a]

	compression	bending	stretch–bend	vdW-1,4	vdW-other	vdW-tot.	torsion	dipole	tot.
				Pt(II) Complexes					
$Pt([12]aneS_4)^{2+}$	0.95	9.73	0.20	0.00	−3.22	−3.22	2.45	−2.73	7.39
$Pt([13]aneS_4)^{2+}$	1.09	9.32	0.23	1.15	−3.21	−2.15	4.06	−2.71	9.93
$Pt([14]aneS_4)^{2+}$	0.87	4.77	0.27	2.42	−4.11	−1.68	1.86	−3.02	3.06
$Pt([15]aneS_4)^{2+}$	0.66	5.21	0.26	4.18	−4.49	−0.31	2.72	−3.08	5.46
$Pt([16]aneS_4)^{2+}$	0.47	5.93	0.25	6.11	−4.76	1.35	3.18	−3.07	8.13
				Pt(IV) Complexes					
$Pt([12]aneS_4)Cl_2^{2+}$	7.80	14.29	0.59	−1.17	0.89	−0.29	9.60	−3.49	28.50
$Pt([13]aneS_4)Cl_2^{2+}$	2.47	11.01	0.41	0.37	−2.16	−1.79	7.54	−3.73	15.92
$Pt([14]aneS_4)Cl_2^{2+}$	1.29	6.56	0.32	1.01	−3.56	−2.46	3.89	−4.03	5.49
$Pt([15]aneS_4)Cl_2^{2+}$	0.72	6.03	0.25	2.71	−5.90	−3.19	2.97	−4.07	2.71
$Pt([16]aneS_4)Cl_2^{2+}$	0.42	6.39	0.21	4.85	−7.14	−2.29	2.41	−4.15	3.01

[a] Energies in kcal mol^{-1}.

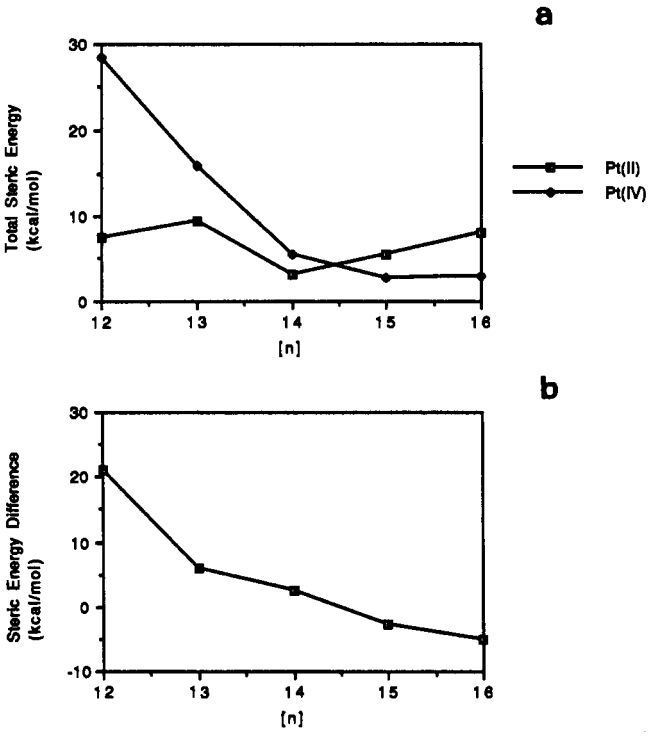

Figure 6. Calculated total steric energy, E_T, of $Pt([n]aneS_4)^{2+}$ (open squares) and $Pt([n]aneS_4)Cl_2^{2+}$ (closed diamonds) (a) and the differences in E_T between the Pt(IV) and Pt(II) complexes (b) as function of ring size (n).

Table V. Atomic Positional Parameters for $[Pt([12]aneS_4)]Cl_2 \cdot H_2O$

atom	x	y	z
Pt1	0.25000	0.25000	0.98186(4)
S1	0.0647(1)	0.1543(1)	0.9391(2)
Cl1	0.25000	0.75000	0.50000
Cl2	0.25000	0.25000	0.4048(3)
C1	0.1197(5)	0.0588(5)	0.7638(6)
C2	−0.0213(5)	0.2763(5)	0.8344(8)
O1	0.1918(5)	−0.0223(4)	1.2572(6)

Table VI. Bond Lengths (Å) and Angles (deg) for $[Pt([12]aneS_4)]Cl_2 \cdot H_2O$

Pt1–S1	2.293(1)	S1–C2	1.818(6)
S1–C1	1.823(5)	C1′–C2	1.532(8)
Pt1–S1–C1	94.6(2)	S1–C1–C2′	107.1(4)
Pt1–S1–C2	100.8(2)	S1–C2–C1′	114.2(4)
S1–Pt1–S1′ (cis)	88.78(4)	C1–S1–C2	104.2(3)

including those of $Pt([14]aneS_4)^{2+}$.[7] In that structure, the conformation of the ligand is similar to that observed in $Pt([12]aneS_4)^{2+}$; i.e., all ligand atoms are located to one side of the S_4 plane. The Pt is 4-coordinate in $Pt([14]aneS_4)^{2+}$, and all four S donor atoms and the central Pt atoms are coplanar; the average Pt–S length is 2.29(1) Å. At the time of this reporting, ensuing

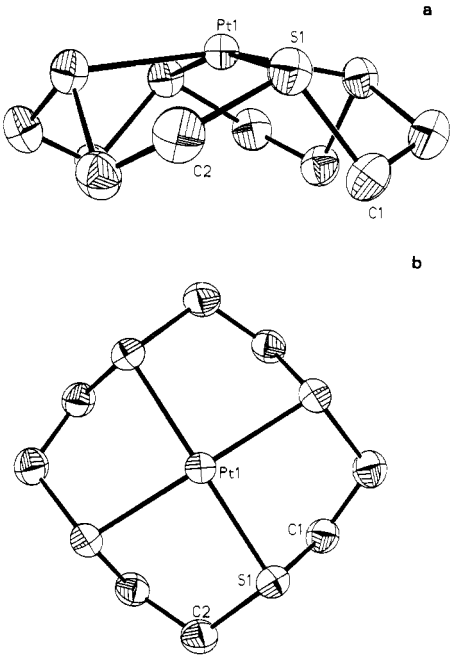

Figure 7. Perspective views of $Pt([12]aneS_4)^{2+}$: side view of the molecule illustrating the folding of the macrocyclic ligand (a), top view (b). Thermal ellipsoids represent 50% probability.

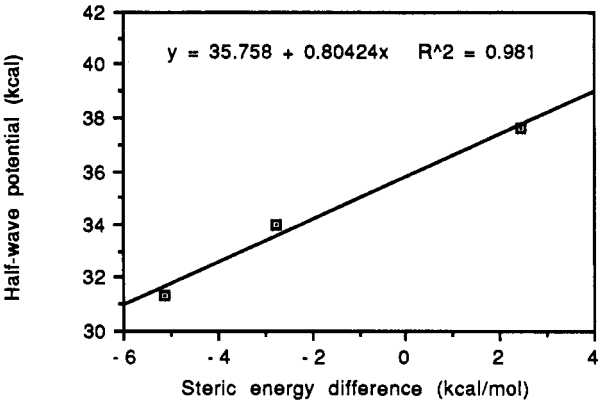

Figure 8. Correlation of variations of half-wave potentials for Pt(II)/Pt(IV) couples with ΔE_T.

discussions focused on the ring size necessary to produce stable 4-coordinate square planar complexes with Pt(II). It was hypothesized that the central cavity of $[13]aneS_4$ and $[12]aneS_4$ macrocycles would be too small for square planar Pt(II) coordination. By analogy with the $Cu([n]aneS_4)^{2+}$ (n = 12–16) studies,[9,16] it was expected that a $[12]aneS_4$–Pt(II) complex would be severely distorted from square planar geometry; perhaps a 2:1

(16) Marsh, R. E. *Acta Crystallogr.* **1986**, *B42*, 193.

Table VII Comparison of Structural Parameters for Macrocyclic Thioether Complexes, $M([n]aneS_4)^{2+}$ [a]

n	Cu–S[b] (Å)	Cu–S–C[b] (deg)	S–Cu–S[b] (deg)	Pt–S (Å)	Pt–S–C (deg)	S–Pt–S (deg)
12	2.33(2)	99(2)	89(5)	2.29(1)[c]	97(3)[c]	88.8[c]
13	2.33	101(4)	89(2)	2.26[d]	103(8)[d]	90(5)[d]
14	2.30	102(2)	90(4)	2.29(1)	104(4)	90(4)
15	2.32	103(3)	90(1)	2.28(1)[d]	111(6)[d]	90(4)[d]
16	2.36	107(4)	90(1)	2.29[d]	117(3)[d]	90(4)[d]

[a] Parameters are averages for each structure (standard deviation for last significant figure is in parentheses); X-ray structures except as indicated. [b] Reference 20. [c] This work. [d] MM2 structure; this work.

macrocycle:Pt *exo* type bonding complex would be generated.[17] However, the structures of the Cu(II) and Pt(II) complexes with $[12]aneS_4$ turn out to be surprisingly similar. Thus, in both complexes the S atoms are arranged in a 3.20-Å square. It is worth noting that the S–S distance in coordinated $[9]aneS_3$ is 3.18–3.20 Å.[18] In the $Cu([n]aneS_4)^{2+}$ complexes, the Cu–S bond length is consistently 2.33 ± 0.03 Å, while, in the X-ray structures of the two $Pt(S_4)^{2+}$ complexes, the Pt–S bond length is 2.29 Å (Table VII). In order to accommodate the 2.33-Å bond length when the S_4 square is 3.20 Å on a side, the Cu atom *must* be 0.55 Å above the S_4 plane. The shorter Pt–S bond only requires a 0.33-Å displacement of Pt from the S_4 plane. It is remarkable that these metals should have so little influence on the stereochemistry of the $[12]aneS_4$ ring. This apparent "rigidity" of $[12]aneS_4$ stands in contrast to the very different ligand conformations found for $Cu^{II}([14]aneS_4)X_2$ and $Pt^{II}([14]aneS_4)$. It appears that the metal with shorter M–S bond "forces" the ligand to fold so that all C atoms are below the S_4 plane. Some of this contrast may be a consequence of the fact that the Cu(II) complex is 6-coordinate. Our MM2 simulations do indicate that 6-coordination (with Cl^-) does tend to flatten the S_4 rings, but our force field does not result in a centrosymmetric structure for the 6-coordinate Pt(IV) complexes.

Comparisons with a variety of structural data indicate that the Pt–S bond is substantially shorter in these thioether complexes than one might have predicted. Thus covalent bonds to S are usually expected to be about 0.27 Å longer than the similar bonds to N (on the basis of covalent radii).[19] The Co–S bond length in $Co([9]aneS_4)_2^{3+}$ is 0.28 Å longer than the Co–N bond length in $Co([9]aneN_4)_2^{3+}$,[18] in excellent agreement with this expectation. Similarly, the Cu–S bond length of 2.30 Å in $Cu^{II}([14]aneS_4)X_2$ is 0.26 Å[20] longer than the 2.04 ± 0.02 Å Cu–amine bond length observed for $Cu^{II}([14]aneN_4)X_2$ complexes. In contrast, the Pt–S bonds in the macrocyclic S_4 complexes[20] are only 0.23 Å longer than the Pt–N bonds in $Pt([14]aneN_4)^{2+}$. The $M([12]aneS_4)^{2+}$ structures are especially important in the comparison of $M([n]aneS_4)^{2+}$ structures, since the M–S bond lengths are not constrained by in-plane ring size effects. Since the Cu–N and Pt–N bond lengths are comparable in cyclic amine complexes, we conclude that the Pt–S bonds are relatively short owing to metal–ligand bonding constraints. The necessity of an extra short bond between the electron-rich Pt(II) and S implies a strong $Pt(d\pi)$-to-$S(\pi)$ back-bonding contribution.

Despite its unusual Pt(II) stereochemistry, $Pt([12]aneS_4)^{2+}$ is a robust material. In addition to its intrinsic interest noted above, the structure of $Pt([12]aneS_4)^{2+}$ is also of value as the only reported $M([12]aneS_4)^{n+}$ X-ray structural determination of high quality, since the $Cu([12]aneS_4)^{2+}$ structure was flawed by disorder and poor crystal quality.

The stereochemical interactions in $Pt([n]aneS_4)^{2+}$ and $Pt([n]aneS_4)Cl_2^{2+}$ complexes can to a reasonable approximation be divided into two classes: (1) interactions between the metal and the sulfur donor atoms; (2) interactions between ligand atoms (including Cl). The second class of interactions dominates the contributions to the MM2-calculated steric energy differences between the $Pt([n]aneS_4)^{2+}$ and the $Pt([n]aneS_4)Cl_2^{2+}$ complexes. The Pt–S interactions can be approximately separated into two categories: (1) steric; (2) electronic. Through the stretching and bonding parameters, the force field which we have used accounts for some of the Pt–S interactions, and it seems appropriate to call this a "steric" component. If the force field were properly parametrized, this steric component would reflect the radial and angular overlap components of the Pt–S bond. The $Pt([n]aneS_4)$ complex structures summarized above may have some unusual features which make them unusually difficult to model. In particular, any angular overlap contribution which originates from the orientation of ligand "nonbonding" orbitals (as for example, π-bonding contributions) is not treated in our force field, since we have ignored any contributions of torsional distortions around the metal.[22,23] Poor metal–sulfur orbital overlap which arises from such misorientation of the ligand orbitals might contribute to the instability of a particular complex, but it would not be treated in our force field. For the present purposes, it is convenient to classify such effects as "electronic".

The misorientation of ligand orbitals is expected to have significant effects on the energies[24-26] and intensities[27] of the ligand field transitions. As can be seen in Table II, the absorption band maxima occur in the same regions of the spectrum for all the complexes of the series. The spectra of $[Pt([12]aneS_4)]X_2$ and $[Pt([13]aneS_4)]X_2$ seem to present the same qualitative features. On the other hand, the spectra of $[Pt([15]aneS_4)]X_2$ and $Pt([16]aneS_4)]X_2$ differ qualitatively from the spectra of the $[12]aneS_4$ and $[13]aneS_4$ complexes, but they are qualitatively similar to one another. The spectrum of $[Pt([14]aneS_4)]X_2$ seems to exhibit characteristics of both of these pairs of complexes. That the electronic spectra of $Pt([n]aneS_4)^{2+}$ complexes with small rings should differ from the spectra of the complexes with large rings is qualitatively in accord with expectation based on the differences in Pt–S bonding stereochemistry. For example, as the ring size increases, the S–Pt–S bond angles progressively approach those expected of a square planar complex, and there is an accompanying decrease in the molar absorptivity of the lowest energy absorption band. Examination of $Pt(N_4)^{2+}$ complexes ($N_4 = (NH_3)_4$, $[14]aneN_4$) and of several $M([9]aneX_3)_2^{m+}$ complexes (X = N, S; M = Pt(II), Pt(III), Ni(II), Co(II), Co(III), Fe(II)) (see Tables II and VIII) indicates that the molar absorptivities of d–d transitions are always much larger in the S- than in the N-bonded complexes. The change in microsymmetry of the Pt center in $Pt([n]aneS_4)^{2+}$ complexes from approximately D_{4h} ($n = 16$) to C_{4v} ($n = 12$) is expected to result in some increase of intensity due to d and p orbital mixing in the lower symmetries. Any systematic changes in ligand π orbital orientation would also be expected to contribute to changes in intensity.

The $M([9]aneX_3)_2^{m+}$ complexes are a useful set of reference

(17) (a) We subsequently found that Schröder[17b] had described a $Pd([12]aneS_4)^{2+}$ structure which had molecular parameters very similar to those of $Pt([12]aneS_4)^{2+}$. A search of the Cambridge database failed to turn up any mention of this structure. (b) Blake, A.; Schröder, M. *Adv. Inorg. Chem.* **1990**, *35*, 2.
(18) (a) Setzer, W. N.; Ogle, C. A.; Wilson, G. S.; Blass, R. J. *Inorg. Chem.* **1983**, *22*, 266. (b) Wieghardt, K.; Küppers, H. J.; Weiss, J. *Inorg. Chem.* **1985**, *24*, 3067. (b) Küppers, H. J.; Neves, A.; Pomp, C.; Ventur, D.; Wieghardt, K., Nuber, B., Weiss, J. *Inorg. Chem.* **1986**, *25*, 2400.
(19) Huheey, J. E. *Inorganic Chemistry*, 2nd ed.; Harper and Row: New York; 1978; p 232.
(20) Rorabacher, D. B.; Jones, T. E.; Ochrymowycz, L. A. *J. Am. Chem. Soc.* **1975**, *97*, 7485 and references herein.
(21) Curtis, N. J. In ref 2, Chapter 4, p 219.
(22) Brubaker, G. R.; Johnson, D. W. *Coord. Chem. Rev.* **1984**, *53*, 1.
(23) (a) Endicott, J. F.; Kumar, K.; Schwarz, C. L.; Perkovic, M. W.; Liu, W.-K. *J. Am. Chem. Soc.* **1989**, *111*, 7411. (b) Schwarz, C. L.; Endicott, J. F. *Inorg. Chem.* **1989**, *28*, 4011. (c) Perkovic, M. W.; Heeg, M. J.; Endicott, J. F. *Inorg. Chem.* **1991**, *30*, 3140.
(24) Larsen, E.; LaMar, G. N. *J. Chem. Educ.* **1974**, *51*, 633.
(25) Schaffer, C. E. *Theor. Chim. Acta* **1974**, *34*, 237.
(26) Lever, A. B. P. *Inorganic Electronic Spectroscopy*; Elsevier: Amsterdam, 1984.
(27) (a) Fenton, N. D.; Gerloch, M. *Inorg. Chem.* **1989**, *28*, 2975. (b) Brown, C. A.; Gerloch, M.; McMeeking, R. F. *Mol. Phys.* **1988**, *64*, 771.

Table VIII.

(a) Absorption Maxima of Charge-Transfer Bands in $M([9]aneS_3)_2^{n+}$ Complexes

M^{n+}	λ_{max} (nm) [ϵ (M^{-1} cm^{-1})]	ref
Pt^{2+}	245 [12 850]; 278 [7000]	31
Pt^{3+}	201 [6600]; 271 [10 000]; 402 [3000]	31
Ni^{2+}	325 [14 000]	17b
Co^{2+}	264 [6500]; 338 [6600]	17b
Co^{3+}	330 [22 000]	17c

(b) Absorption Maxima of d–d Transitions in $M([9]aneS_3)_2^{n+}$ and $M([9]aneN_3)_2^{n+}$ Complexes

Complex	λ_{max} (nm) [ϵ(M^{-1} cm^{-1})]	ref
$Pt([9]aneS_3)_2^{2+}$	432 [95]	31
$Ni([9]aneN_3)_2^{2+}$	308 [12]; 505 [5]; 800 [7]; 870[sh] [a]	28
$Ni([9]aneS_3)_2^{2+}$	527 [26]; 784 [27]	17b
$Co([9]aneN_3)_2^{3+}$	333 [89]; 458 [100]	29
$Co([9]aneS_3)_2^{3+}$	476 [320]	17c
$Co([9]aneN_3)_2^{2+}$	318[sh]; 462 [5.9]; 545[sh]; 630 [1.4]; 850 [2.4]	30
$Co([9]aneS_3)_2^{2+}$	480 [92]; 560[sh]; 730 [11]	17b
$Fe([9]aneN_3)_2^{2+}$	288 [560]; 387 [17]; 601 [6]	30
$Fe([9]aneS_3)_2^{2+}$	395 [52]; 523 [53]	17b

[a] Shoulder; peak not resolved.

compounds.[17,28-31] The d–d absorptions of the Ni(II) complexes occur at slightly higher energy for the sulfur than for the nitrogen donor ligands (see Table VIII).[17b,28] This order is reversed for the Co(III) complexes.[17c,29] A ligand field analysis[26] of these spectra results in values of $10Dq = 12.50 \times 10^3$ and 12.76×10^3 cm^{-1}, respectively, for the N and S donors on Ni(II).[32] For the Co(III) complexes, the respective values of $10Dq$ are 22.897×10^3 and 22.00×10^3 cm^{-1}.[33] If we adopt the angular overlap model of parametrization of $10Dq$ into σ (ϵ_σ) and π (ϵ_π) contributions[24-26] ($10Dq = \epsilon_\sigma - 4\epsilon_\pi$), then the most straightforward interpretation of the spectroscopy of these $M([9]aneX_3)_2^{n+}$ complexes is that the π contributions of the S donor are relatively more significant for Ni than for Co (i.e., that $\epsilon_\pi/\epsilon_\sigma$ is larger for Ni(II) than for Co(III)) and that the π contributions to M–X bonding are attractive ($\epsilon_\pi < 0$). With these relatively electron-rich metals, this implies a dominant back-bonding contribution to ϵ_π. For complexes which have very similar structures, the importance of back-bonding should increase with the increasing ease of ionization of electrons in the metal dπ orbitals.

If metal dπ to ligand X π back-bonding interactions are a truly important feature of metal–thioether complex stability, then one would expect to find some spectroscopic manifestations of an acceptor orbital on the S donor. Ligand to metal and metal to ligand charge-transfer (LMCT and MLCT) absorption maxima should vary approximately in proportion to the sum of the thermodynamic energy difference ($\Delta E_{1/2}$) for transferring charge from the donor to acceptor, plus a nuclear reorganizational term (λ), which increases with increasing differences in the molecular structures of the ground state and the CT excited state. The lower energy CT bands of $Co([9]aneS_3)_2^{2+}$ and $Ni([9]aneS_3)_2^{2+}$ are most plausibly assigned as MLCT transitions, since the cobalt complex is 0.4 V more easily oxidized but is expected to have a somewhat larger value of λ than the Ni complex. Similar reasoning suggests that the lowest energy transitions for $Co([9]aneS_3)_2^{3+}$ and $Pt([9]aneS_3)_2^{3+}$ are LMCT absorptions (one expects a substantially larger value of λ for the reduction of Co(III) and the oxidation of Pt(III) than for the reduction of Pt(III)). Thus, the spectroscopy indicates, not unreasonably, that the thioether ligands can function as either donors or acceptors, although the acceptor properties seem to be most important in stabilizing low-valence states of metals.[6] Reorganizational parameters evaluated for the LMCT transitions in $Co([9]aneS_3)_2^{3+}$ and $Pt([9]aneS_3)_2^{3+}$ can be combined with the MLCT band of $Co([9]aneS_3)_2^{2+}$ to predict a LMCT transition at about 422 nm in $Pt([9]aneS_3)_2^{2+}$. A weak transition at 432 nm, observed for this complex, has been assigned as a d–d transition.[31] The lowest energy d–d transitions that we have been able to resolve in the $Pt([n]aneS_4)^{2+}$ complexes occur between 340 and 315 nm, and all of these bands are more intense than that for the transition reported for $Pt([9]aneS_3)_2^{2+}$. The intensities could relate to the angular overlap issues which have been raised above; however, the low intensity would argue for relatively good angular overlap, so that the energy would be even more anomalous for a d–d transition. The contrast with the d–d transitions of amine complexes is also striking (see Table II) and would require about a 10×10^3 cm^{-1} smaller value of $10Dq$ (and a 2–5 times smaller than expected intensity) for the S than for the N donor ligands. We suspect that the 432-nm transition of $Pt([9]aneS_3)_2^{2+}$ is a very weak MLCT transition. If this argument is correct, the small intensity of this transition would have to be attributed to poor overlap between the Pt d_{z^2} donor orbital and the S acceptor orbitals in the nearly square planar complex.

In view of the considerations outlined above, we attribute the lowest energy absorption bands in the $Pt([n]aneS_4)^{2+}$ complexes to predominantly d–d transitions. That the intensities of these transitions increase as n decreases is consistent with the increasing deviation from a simple square planar microenvironment. These distortions could also promote mixing of d–d and MLCT states. A standard angular overlap treatment of the shifts in absorption maxima, expected for the variations in S–Pt–S and Pt–S–C angles, is consistent with the trends in maxima ($Pt([14]aneS_4)^{2+}$ at the highest energy) of the lowest energy absorption bands only if there are very large ϵ_π contributions to the orbital energies. The magnitudes of these effects are difficult to predict in the absence of knowledge of the spatial properties of the acceptor orbitals.[34] A large-amplitude (10–30°) misalignments of this orbital would be compatible with the observations.

As can be seen in Figure 6a, the calculated steric energies of Pt(II) complexes seem to vary according to two opposite trends: (1) for a large metal ion, five-membered chelate rings result in less strain than 6-membered;[35] (2) more 6-membered chelate rings induce a larger ring size and, thus, less strain for a large metal ion. Our MM2 calculations show that the steric energies of the Pt(IV) complexes vary systematically with ring size (Figure 6a). The trend, toward greater interligand repulsions as ring size decreases, is in accord with intuitive expectation based on the structure of the complexes.[7] Since the calculated steric energies of the Pt(II) complexes do not vary a great deal (E_T(av) = 6.8 ± 2.6 kcal mol^{-1}), the difference between steric energies calculated for $Pt([n]aneS_4)Cl_2^{2+}$ and $Pt([n]aneS_4)^{2+}$, ΔE_T, also decrease in a systematic manner with increasing n (Figure 6b). The measured values of $E_{1/2}$ for the complexes with n = 14–16 correlate reasonably well with ΔE_T (Figure 8). We were unable to determine half-wave potentials for the complexes with [13]$aneS_4$ and [12]$aneS_4$ ligands ($E_{1/2} \geq 0.9$ V); extrapolation of the plot in Figure 8 would predict $E_{1/2} \cong 0.9$ and 1.1 V, respectively, vs

(28) Yang, R.; Zompa, L. J. *Inorg. Chem.* **1976**, *15*, 1499.
(29) Koyama, H.; Yoshino, T. *Bull. Chem. Soc. Jpn.* **1972**, *45*, 481.
(30) Wieghardt, K.; Schmidt, W.; Hermann, W.; Küppers, H. J. *Inorg. Chem.* **1983**, *22*, 2953.
(31) Schröder, M. *Pure Appl. Chem.* **1988**, *60*, 517.
(32) Based on the following:[26] $E(^3T_2) - E(^3A_2) = 10Dq$; $E(^3T_1) \sim E(^3A_2) = 2.5B + 15Dq - 0.5x$; $E(^3T_1') - E(^3A_2) = 2.5B + 15Dq + 0.5x$; $x = [225B^2 + 100Dq - 180\ DqB]^{1/2}$. Values of B = 980 and 680 cm^{-1} were obtained for the respective complexes.
(33) Based on the following:[26] $E(^1T_1) - E(^1A_1) = 10Dq - C + 86B^2/10Dq$; $E(^1T_2) - E(^1A_1) = 16B - C + 2B^2/10Dq$. Assuming $C \cong 4B$, $B \cong 590$ cm^{-1} for the N donor ligand. Values of B = 410–590 cm^{-1} gave nearly the same value of $10Dq$ for the S donor ligand.
(34) On the basis of a SF_4-like model for the coordinated S, one could argue for a π-type acceptor orbital approximately orthogonal to one of the Pt–S–C planes and lying more or less in the other. This model, would place two S atom "lone pairs" and one C–S bond in a trigonal plane, with one of these "lone pairs" being used for dative bonding to Pt. This crude model is reasonably consistent with the paired clustering of Pt–S–C angles (100–104 and 106–120°) and the 98–100° C–S–C angles in these complexes.
(35) Hancock, R. D. *Acc. Chem. Res.* **1990**, *23*, 253 and references herein.

Ag/AgCl. The slope of the correlation line in Figure 8 is 0.8, indicating that the steric energy as evaluated by our force field is the major factor in determining $E_{1/2}$ but that it is probably not the only factor. As noted above, the force field parametrization which we have used neglects electronic contributions which can be considered to arise from variations in the angular orbital overlap between the Pt and S. The spectroscopy of these complexes indicates that variations in orbital angular overlap are significant. However, the spectroscopy does not directly bear on the effects of these variations on the ground state stabilization energies of the Pt(II) or of the Pt(IV) complexes. The correlation in Figure 8 indicates that there is a small "electronic" contribution, about 20%, to the free energies of the Pt(II) and Pt(IV) ground electronic states. Overall, the present work supports our previous hypothesis[7] that variations in inter- and intraligand steric energies account for the dominant trends in Pt(II)–Pt(IV) electrochemistry.

One of our original motivations for study of platinum(II)–macrocycle complexes was to find systems which would make formation of Pt(IV) relatively difficult without eliminating potential Pt coordination sites. The [12]aneS$_4$ ligand system seems to have many of the desired structural features, and we would expect some axial ligands to stabilize the [12]aneS$_4$–Pt(III) complexes with respect to disproportionation. However, we have so far found no axial ligand which in combination with the [12]aneS$_4$ ligand thermodynamically stabilizes Pt(III) with respect to Pt(II) and Pt(IV). Some kinetic stabilization seems plausible, but this issue will have to be considered elsewhere.

Acknowledgment. We gratefully acknowledge partial support of this research by the Division of Chemical Sciences, Office of Basic Energy Sciences, Office of Energy Research, U.S. Department of Energy. M.A.W. thanks the Région Rhône-Alpes, France, for fellowship support. The X-ray diffractometer used herein was purchased through an NSF grant to Wayne State University. We are also grateful for partial support of the research at the University of Wisconsin—Eau Claire by the Research Corp. and by the donors of the Petroleum Research fund, administered by the American Chemical Society. We are very grateful to Ms. Isabel Moy Chan for synthesizing several of the ligands used in this work.

Supplementary Material Available: Table S-1, giving molecular mechanics input parameters, Tables S-II and S-III, comparing the calculated and observed bond lengths and angles for Pt([12]aneS$_4$)$^{2+}$ and Pt([12]aneS$_4$)$^{2+}$, Tables S-IV–S-VI, giving supplemental crystallographic data, thermal parameters, and hydrogen atomic parameters for [Pt([12]aneS$_4$)]Cl$_2$·H$_2$O, Figures S-1–S-4, showing the visible–UV spectra of the Pt([n]aneS$_4$)$^{2+}$ complexes in water for n = 12, 13, 15, and 16, respectively, and a list of references for the supplementary material (10 pages). Ordering information is given on any current masthead page.